Received: 23 March 2021 | Revised: 29 October 2021 | Accepted: 16 November 2021

DOI: 10.4218/etrij.2021-0038

ORIGINAL ARTICLE

ETRI Journal WILEY

Performance analysis of DSSS- and CSS-based physical layer for IoT transmission over LEO satellites

Sooyeob Jung[1,2] | **Gyeongrae Im[2]** | **Dong-Hyun Jung[2]** | **Pansoo Kim[2]** | **Joon Gyu Ryu[2]** | **Joonhyuk Kang[1]**

[1]Department of Electrical Engineering, Korea Advanced Institute of Science and Technology, Daejeon, Republic of Korea

[2]Satellite Wide-Area Infra Research Section, Electronics and Telecommunications Research Institute, Daejeon, Republic of Korea

Correspondence
Sooyeob Jung, Department of Electrical Engineering, Korea Advanced Institute of Science and Technology. Daejeon, Republic of Korea.
Email: jung2816@kaist.ac.kr

Funding information
Institute of Information and Communications Technology Planning and Evaluation, Grant/Award Number: 2020-0-00843

Correction added on 20th April 2022, after first online publication: the author Sooyeob Jung affiliations have been updated.

Abstract

To determine a suitable waveform for Internet of Things (IoT) transmission over low-Earth orbit (LEO) satellites, this paper reports the results of a performance comparison between chirp spread spectrum (CSS)-based LoRa and direct sequence spread spectrum (DSSS)-based Ingenu. The performance of both waveforms was measured in terms of the packet error rate, throughput, and packet loss rate, considering the Doppler effect caused by the high speed of LEO satellites and the interference among multiple terminals. Simulation results indicate that the DSSS scheme is more suitable than the CSS scheme for high-traffic IoT services because of its robustness against interference among multiple terminals. However, the CSS scheme is more suitable than the DSSS scheme for high-mobility IoT services because of its robustness against the Doppler effect. We discuss various solutions, such as the preprocessing of Doppler effect and avoidance of packet collision, to enhance the performance of the DSSS and CSS schemes. The simulation results of the proposed solution show that the enhanced DSSS scheme can be a proper waveform in IoT transmission over LEO satellites for both the high-traffic and high-mobility services.

KEYWORDS

CSS, Doppler effect, DSSS, Ingenu, interference, IoT, LEO satellite, LoRa, unlicensed band

1 | INTRODUCTION

The concept of the Internet of Things (IoT) has revolutionized our lives and many industries. Today, connected devices take charge of much of our daily lives. In industry, the monitoring of remote sensors and assets is increasingly required to reduce operational costs and increase productivity in various areas, such as smart agriculture, public utilities, and fleet tracking. It is also certain that the IoT will play a key role in the evolution toward future wireless communication.

Connected devices can be deployed in either licensed or unlicensed bands, such as the industrial, scientific, and medical bands and TV white space, respectively. For licensed bands, narrowband IoT (NB-IoT) [1], created by the 3rd Generation Partnership Project (3GPP), is the representative IoT standard, and it is able to use the infrastructure of conventional 3GPP networks, such as 2G, 3G, and 4G. For unlicensed bands, low-power wide-area (LPWA) networks, such as LoRa [2], Sigfox [3], and Ingenu [4], are widely deployed for specific IoT services. However, some particular services in rural and remote areas, such as marine services, air travel, oil and gas, and remote farming, will require satellite links that can offer global coverage. Unlike the satellite networks, the terrestrial wireless networks are challenging to expand the service range owing to the technical problems and lack of a revenue model. Especially, densely deploying base stations on the ocean is difficult and requires the multihop systems using vessels and unmanned aerial vehicles (UAVs). However, IoT transmission over low-Earth orbit (LEO) satellites has being proposed as the commercial solutions from several global satellite companies, such as Starlink by SpaceX, Telesat, and Kuiper by Amazon. Cost-effective and easy-to-deploy large-scale satellite networks are being established. In the 1990s, the conventional companies, such as Iridium, Globalstar, and Orbcomm, tried to provide global connectivity [5]. However, most of them failed owing to financial problems. However, satellite technology has considerably evolved over the past 20 years, and companies have developed creative business model that generate revenue from connections. Additionally, the huge capital of companies and investors now has room to invest in the satellite industry.

LEO satellite communication systems can be used to interoperate in hybrid terrestrial-satellite systems. They have shorter transmission delay and lower path loss than geostationary Earth orbit (GEO) satellite systems having the cost burden of high capital expenditure (CAPEX) and operational expense (OPEX). These properties can lead to the low-power consumption, long battery life, low launch costs, and simple antenna designs. Therefore, LEO satellites are regarded as the leading candidate to achieve seamless global communication services. Recently, 3GPP has performed standardization related to nonterrestrial networks (NTNs) to integrate satellites based on a LEO constellation into the 5G network [6]. However, IoT waveforms, such as LoRa, Sigfox, Ingenu, and NB-IoT, are not straightforwardly applicable over LEO satellites owing to the Doppler effect caused by the high speed of such satellites and the interference among multiple terminals [7]. Compared with the terrestrial IoT services having the operating range from a few kilometers in urban areas to over 10 km in rural areas, the beam coverage of LEO satellites may range from tens of kilometers to a few thousands of kilometers and such wide coverage increases largely the number of simultaneous access terminals. Managing the strong interference is a critical issue in IoT-over-satellite communication system. Moreover, the system may suffer from a large and time-variant frequency shift owing to the Doppler effect.

This paper analyzes the performance of IoT transmission in environments with interference caused by packet collisions by considering unslotted ALOHA-based random multiple access [8]. In random multiple access schemes, different users do not access the same channel or access it with very limited coordination, which can lead to packet collisions. In contrast to demand assignment multiple access schemes, which avoids collisions by allocating radio resources to users in advance, in random multiple access protocols, packet collisions cannot be avoided owing to the lack of coordination. These uncoordinated multiple access protocols are preferable over scheduled access in IoT transmission scenarios over LEO satellites because of their long inherent feedback delay, large user population, and sporadic user activity patterns. In unslotted ALOHA schemes, we particularly focus on spread spectrum technologies, including LoRa based on the chirp spread spectrum (CSS) and Ingenu based on the direct sequence spread spectrum (DSSS), which have the link budget advantage. Among LPWA networks, NB-IoT shows the most superior link budget. Next, Ingenu, LoRa, and Sigfox follow sequentially. However, this paper excludes NB-IoT and Sigfox from the primary competitor for IoT-over-satellite owing to several reasons. NB-IoT has the issues of cost, power, and priority in spite of the low latency and high throughput. The spectrum costs are incurred using licensed bands and the terminals have a problem of the high cost and short battery life. Moreover, it has a low priority in a cellular network giving preference to voice and data during on-peak times. Sigfox has a very low complexity and costs owing to the simplistic nature of the protocol. However, it transmits at the lowest data rate and has the communication capability limitations based on its one way, unacknowledged, and fixed packet data model. In addition, it will face the severe interference problem by wideband signals because a wideband signal is capable of destroying the entire band while wiping out thousands of narrowband channels. However, the large link budget of Ingenu and LoRa enables very long-range transmission. In addition, they benefit in terms of total cost of ownership (TCO) and link capability. TCO includes network costs, spectrum costs, endpoint costs, and battery costs. Link capability includes uplink throughput, downlink capability, robustness, and priority [9,10]. Many studies have reported that the LoRa physical layer has limitations on multiple access. However, the performance and capability can be improved by the quality of media access control (MAC) implementation [11], and there is a lot of room for improvement in the physical layer [12,13]. Therefore, we analyzed LoRa as well as Ingenu for IoT transmission services over LEO satellites.

Until now, the comparative studies on the performance of LPWA technologies in both terrestrial and satellite networks have been insufficient because each scheme uses a proprietary protocol and the transmission characteristics are different [10]. The spread spectrum technologies analyzed in this paper are also difficult to compare the physical layer performance. In general, the throughput is measured on MAC load for DSSS scheme and on channel occupancy for CSS scheme.

The main contributions of the paper can be summarized as follows:

1. We analyze the performance in terms of the packet error rate (PER), throughput, and packet loss rate (PLR) by matching the evaluation indicators of DSSS and CSS equally in the realistic LEO channel model that reflects multiple access and Doppler effect. Through a performance comparison, we can find an efficient IoT transmission protocol for fulfilling various user requirements in LEO satellite communication systems.
2. We also propose various solutions to improve the throughput performance, including the enhancement on physical layer, eliminating the Doppler effect, and using multiple spreading factors (SFs). In particular, it is applied the beacon-based precompensation schemes that does not use a GPS module by using two look-up tables (LUTs) to recover the Doppler effect in DSSS transmission. This scheme shows the low-power consumption and precise estimation performance. Additionally, an optimization problem solver can be used to enhance the existing CSS scheme using multiple SFs with equal probability. The improved throughput of the proposed schemes is compared with the state-of-the-art IoT transmission schemes, especially in low-traffic region.

The remainder of this paper is organized as follows. The candidate IoT waveforms are outlined in Section 2. In Section 3, the channel model and link budget are analyzed for IoT transmission over LEO satellites, and a performance comparison between two IoT transmission schemes is undertaken. In Section 4, an enhanced IoT transmission scheme is suggested on the basis of simulation results. Some concluding remarks are made in Section 5.

2 | CANDIDATE WAVEFORMS FOR SATELLITE IOT

2.1 | Direct sequence spread spectrum

DSSS is a spectrum modulation technique given in the IEEE 802.15.4k standard for low-energy critical infrastructure monitoring (LECIM) [4]. Ingenu provides a terrestrial IoT service under the name of random phase multiple access (RPMA) [14] that uses DSSS for LPWA networks and is based on slotted ALOHA. The frame structure of the IEEE 802.15.4k DSSS physical layer is elaborately illustrated [4]. As shown in Figure 1A, the transmitter exploits the differential binary phase-shift keying (D-BPSK) modulation and convolutional encoding to endure very low signal-to-noise ratio (SNR) and strong co-channel interference.

The receiver structure for DSSS is presented in Figure 1B. As a first step, preamble detection is performed to estimate the start of a packet prior to timing recovery and frequency estimation. In this paper, as suggested in Kim and others [15], a simple preamble detector using partial correlators and multiplication operators is applied to reduce complexity. After preamble detection, coarse synchronization and fine synchronization are sequentially performed to recover the phase offset, Doppler shift, and signal level offset. After synchronizing and estimating the start point, the remaining processes such as de-spreading, differential decoding, de-interleaving, and convolutional decoding are performed in succession.

Although the DSSS scheme is strong against co-channel interference due to packet collision, it is very weak against Doppler shift due to the high speed of LEO satellites, so that the initial preamble detection probability is greatly reduced.

2.2 | Chirp spread spectrum

CSS is a spectrum modulation technique [16] for the LoRa waveform, patented by Semtech. LoRa has a large communication link budget owing to the high receiver sensitivity. This enables very long-range transmissions. In addition, this transmission scheme provides the

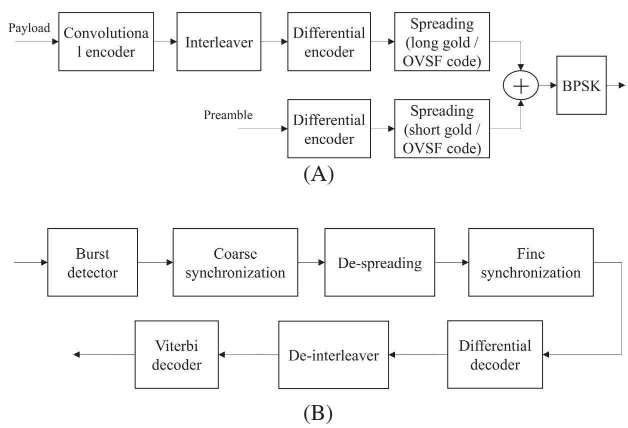

FIGURE 1 (A) Transmitter and (B) receiver structure of direct sequence spread spectrum (DSSS) transmission scheme

scalable bandwidth and robustness against channel distortion, such as Doppler effect, fading, and multipath. However, the LoRa physical layer has limitations on multiple access owing to the nonorthogonal arrangement among CSS signals with the same SF. To solve this problem, CSS signals with different SFs can be transmitted in unslotted ALOHA channels, and various studies on physical layers, such as symmetric CSS [12] and asymmetric CSS [13] are in progress to endure the interference among multiple terminals. Moreover, the performance and capability can be improved depending on the quality of MAC implementation, and many LoRa network protocols, such as LoRaWAN, Symphony Link, and MAC on Time, have been proposed [11].

The physical layering principle of CSS-based LoRa is described in Ferré and Giremus [17]. A set of consecutive SF bits makes up one symbol, one symbol is spread across 2^{SF} chips, and the information that the SF bits imply is expressed as a cyclic shift of the modulated chirp symbol. A chirp sign with a continuously increasing frequency is called an up-chirp, whereas a chirp sign with a continuously decreasing frequency is called a down-chirp. Figure 2A presents the structure of the LoRa transmitter. The transmitter performs hamming coding, diagonal interleaving, gray to binary mapping, and CSS modulation to generate LoRa packets.

The receiver structure for CSS-based LoRa is suggested in Figure 2B. For all input samples, the discrete Fresnel transform (DFnT) is used to find the preamble start position. After preamble detection, synchronization including timing recovery and frequency estimation is performed using the DFnT result. Binary to gray de-mapping, diagonal de-interleaving, and hamming decoding are successively performed for synchronized samples as shown in Figure 2B [18].

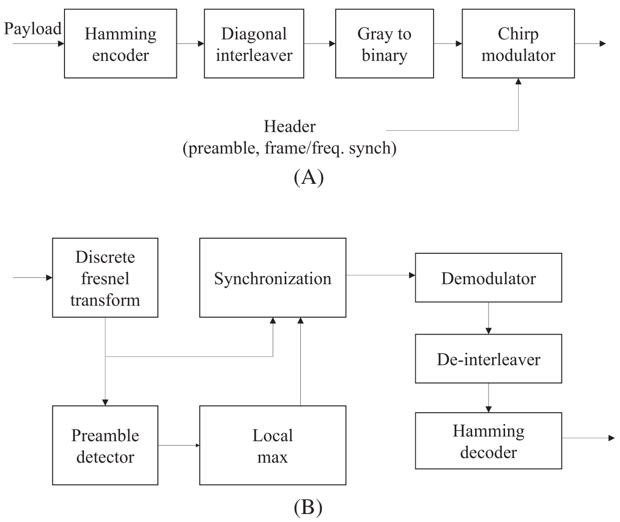

FIGURE 2 (A) Transmitter and (B) receiver structure of chirp spread spectrum (CSS) transmission scheme

3 | PERFORMANCE EVALUATION AND COMPARISON FOR SATELLITE IOT WAVEFORMS

3.1 | LEO satellite channel model

For our satellite IoT scenario, we adopted the unslotted ALOHA MAC protocol, which does not require network timing synchronization for random access channels. In Chan and others [5], such the IoT-over-satellite communication system using a shared spectrum was evaluated the performance in terms of coverage availability and signal quality through a reliable and robust analytical model. In the performance modeling framework, the satellite channel and interference model are obtained from the geometric model using orbital data. The various system parameters of LEO satellite channel model are shown in Table 1 [5,19,20]. These parameters are based on the IoT NTN reference scenario and EU regulations. Specially, EU regulations stipulate that the effective radiated power (ERP) under 25 mW in 900 MHz frequency must be supported. This ERP value can be converted into the effective isotropic radiated power (EIRP) of 16 dBm. This paper follows mainly the performance modeling framework of [5] with NTN scenario and EU regulations.

From the satellite altitude H_{s}, the Earth's radius R_{E}, relative latitude γ, and relative longitude ψ, satellite coordinates are $S=(R_{\mathrm{E}}+H_{\mathrm{s}}, 0, 0)$ and the terminal coordinates are $T=(R_{\mathrm{E}}\cos\gamma\cos\psi, R_{\mathrm{E}}\cos\gamma\sin\psi, R_{\mathrm{E}}\sin\gamma)$. The elevation angle θ can be obtained by

TABLE 1 System parameters

Parameters	Value
Maximum Tx EIRP	14 dBm
Antenna gain	12 dBi
Satellite frequency	900 MHz
Satellite altitude	600 km
Minimum elevation angle	20°
Maximum distance	1392 km
Free-space path loss	154.3 dB
Atmospheric loss	0.1 dB
Noise figure	6 dB

Abbreviations: EIRP, effective isotropic radiated power.

$$\theta = \arcsin\left(\frac{\overrightarrow{OT}\cdot\overrightarrow{TS}}{\left\|\overrightarrow{OT}\right\|\cdot\left\|\overrightarrow{TS}\right\|}\right), \tag{1}$$

where O is the center of the Earth. $\|\cdot\|$ and $\vec{\cdot}$ denote the Euclidean norm and the Euclidean vector, respectively. The normalized Doppler shift $\Delta f/f$ [21] can be calculated by

$$\frac{\Delta f}{f} = -\frac{R_E R w_F \sin(\psi)\cos(\Delta\theta)}{c\sqrt{{R_E}^2 + R^2 - 2R_E R\cos(\psi)\cos(\Delta\theta)}}, \tag{2}$$

$$\Delta\theta = \arccos\left[\frac{R_E}{R}\cos(\theta_{\max})\right] - \theta_{\max}, \tag{3}$$

$$w_F = w_S - w_E\cos(i), \tag{4}$$

where R is the distance between the center of the Earth and satellite, $\theta_{\max}$ is the maximum elevation angle corresponding to $\psi = 0$, c is the speed of light, w_F is the angular velocity of the satellite rotation in the Earth-centered fixed (ECF) frame, w_S is the angular velocity of the satellite rotation in the Earth-centered inertial (ECI) frame, $2\pi/T$, w_E is the angular velocity of the Earth's rotation in the ECF frame, $2\pi/(3600\times 24)$, and i is the inclination angle of the orbit. As shown in Figure 3A, the beam coverage from LEO satellite is composed of lots of cell coverages. In this paper, each cell is defined by shifting at regular intervals the latitude and longitude, and then the normalized Doppler shift per cell can be calculated from (2). The IoT terminals are located in the cell coverages and are uniformly distributed under the LEO satellite beam.

The interference model is illustrated in Figure 3B. The input signal in the receiver induces overlapping bursts by unslotted ALOHA MAC protocol, under the following assumptions. First, considering the total number of IoT terminals and the amount of traffic per cell, which is assumed to follow a Poisson distribution, are denoted as N_T and ε, respectively, the average number of transmission signals from IoT terminals in the detection window of a gateway demodulator corresponds to εN_T. Therefore, the average number of overlapping packets in a detection window is $2\varepsilon N_T$. Then, the time of packet emission (TOE) d_k is determined by a discrete uniform distribution probability condition in a transmission window L. In fact, one LEO satellite covers an area of several tens of square kilometers, much greater than the area of terrestrial gateways, considerably increasing the probability of packet collisions at the receiver in an uplink channel.

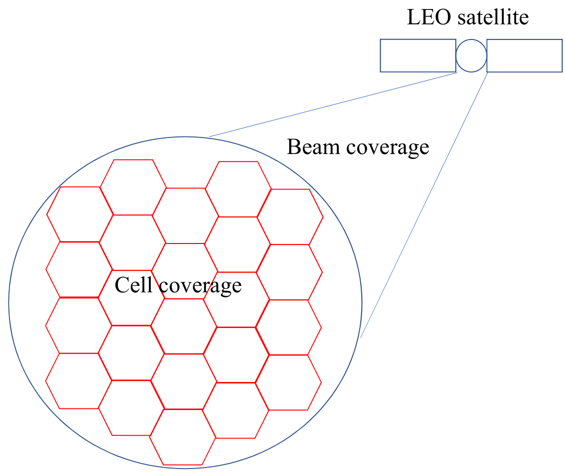

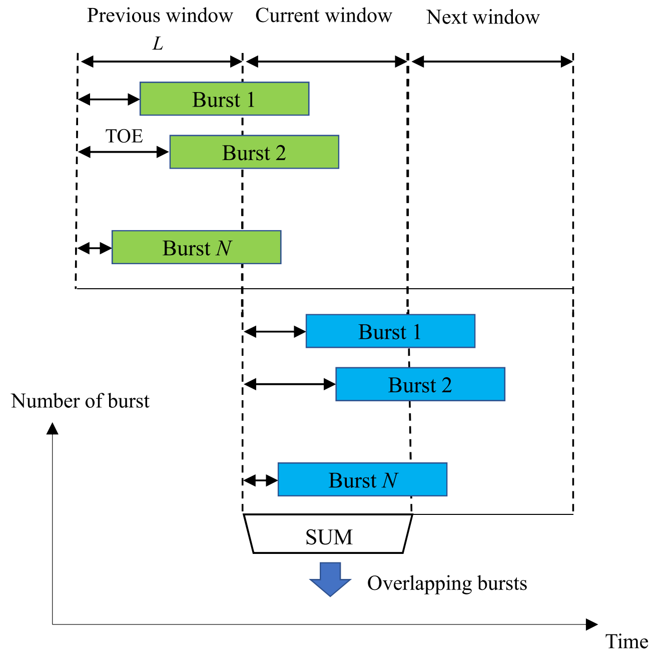

FIGURE 3 (A) Low-Earth orbit (LEO) satellite and (B) traffic generation

In the satellite channel models [22,23] that have the dominant direct signal, a line-of-sight component, the Rician fading is commonly considered. In addition, shadowing in the large-scale fading provokes the attenuation of the direct signal by buildings, trees, hills, and mountains. However, the small-scale fading including the Doppler spread and multipath delay spread has little effect in satellite IoT scenario of this paper. The Doppler spread related to the motion of the terminal is tiny compared with the Doppler shift caused by the relative motion of the satellite. The delay spread induces only the slight intersymbol interference owing to IoT applications

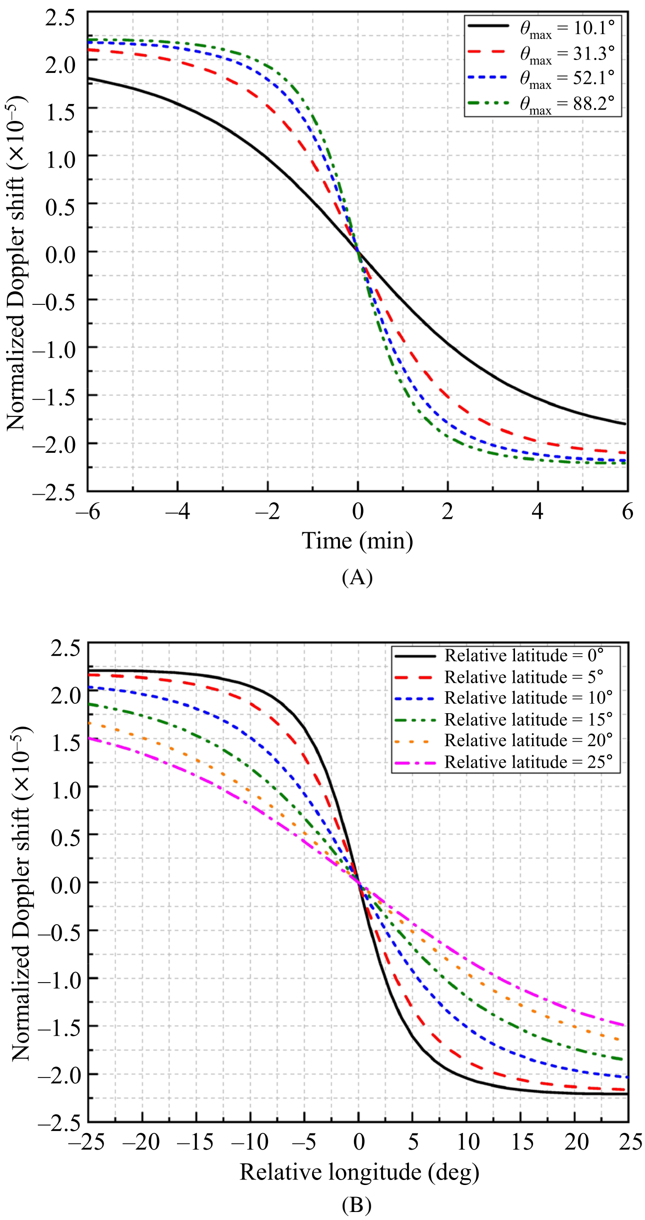

FIGURE 4 Normalized Doppler shift with (A) time and (B) relative longitude in altitude 600 km and inclination angle 52°

with the low symbol rate. Therefore, this paper does not consider the delay spread and Doppler spread. As a result, the channel can be modeled as additive white Gaussian noise (AWGN) with the effect of shadowing, Rician fading, and Doppler shift. The received signal at time t by the kth terminal can be expressed as follows:

$$r_k(t) = a_k s_k(t - d_k) e^{j(2\pi f_{dk} t + \theta)} + w_k(t), \tag{5}$$

where $s_k(t)$ is the signal transmitted from the IoT terminal, $w_k(t)$ is the AWGN, a_k is the magnitude, d_k is the TOE, θ is the phase offset, and f_{dk} is the normalized Doppler shift in (2), which is large and time variant based on the position of the LEO satellite. A verification of the Doppler shift calculation is provided in Figure 4. In Figures 4A and 4B, the normalized Doppler shift curves for maximum elevation angles ranging from 10.1° to 88.2° and relative latitudes ranging from 0° to 25° are shown in relation to time and relative longitude, respectively. These curves are symmetrical to the negative values of the maximum elevation angles and the relative latitudes. In addition, the log-normal shadowing is added to a_k. The shadowing attenuation in signal power is $-\xi$ dB, which is zero mean Gaussian with variance σ^2. By Rician fading, the power distortion and phase distortion with K factor is reflected on a_k and θ, respectively [16].

3.2 | Sensitivity and link budget

LPWA network technologies in terrestrial IoT can be applied to IoT transmission via LEO satellites by considering additional channel elements for satellite communication. In order to determine whether waveforms previously designed for terrestrial IoT are applicable to satellite IoT communication, it is necessary to calculate the link budget considering satellite channel conditions. Considering a free-space path loss, the distance at which the transmitter and the receiver can communicate depends on several factors, which can be summarized by the basic form of the Friis transmission equation. The Friis equation is given by [24]:

$$P_r = P_t G_t G_r \left(\frac{\lambda}{4\pi d}\right)^2, \tag{6}$$

where P_t and P_r are the power at the transmitter and receiver, respectively; G_t and G_r are the antenna gain of the transmitter and receiver, respectively; λ is the wavelength of the signal transmitted; and d is the distance between the transmitter and the receiver.

To compute the link budget for system design, the sensitivity P_{req}, which is the minimum received signal power required to achieve an arbitrary level of error, can be obtained by the following equation [24]:

$$P_{req} = \mathrm{SNR}_{req} + N_0 + 10\log_{10} B + N_F, \tag{7}$$

where SNR_{req} is the required SNR for the target performance, N_0 is the noise power spectral density, B is the bandwidth, and N_F is the noise figure. Generally, N_0 is considered to be -174 dBm, which is its value at $T = 288$K (15°C). Using the parameters shown in Table 1, P_r can be obtained as -128.51 dBm. P_{req} can be obtained on the basis of the detailed specifications of the

TABLE 2 Simulation environments

Parameters/ scheme	DSSS	CSS
Bandwidth	300 kHz	300 kHz
Code rate (r)	Convolutional code 1/2	Hamming code 1/2
Modulation	D-BPSK	CSS modulation
Symbol rate	0.976 ksps	61 sps
Chip rate	250 kcps	250 kcps
Spreading factor (SF)	8[a]	12
Payload length	100 bits	100 bits
Header length	40 bits	12 bits
E_b/N_0	7 dB	8.34 dB
E_c/N_0	−20 dB	−20 dB

Abbreviations: CSS, chirp spread spectrum; D-BPSK, differential binary phase-shift keying; DSSS, direct sequence spread spectrum.
[a]SF in Ingenu defines generally the number of chips per bit. However, this paper follows equally the SF representation, exponent, in LoRa to clear the confusion.

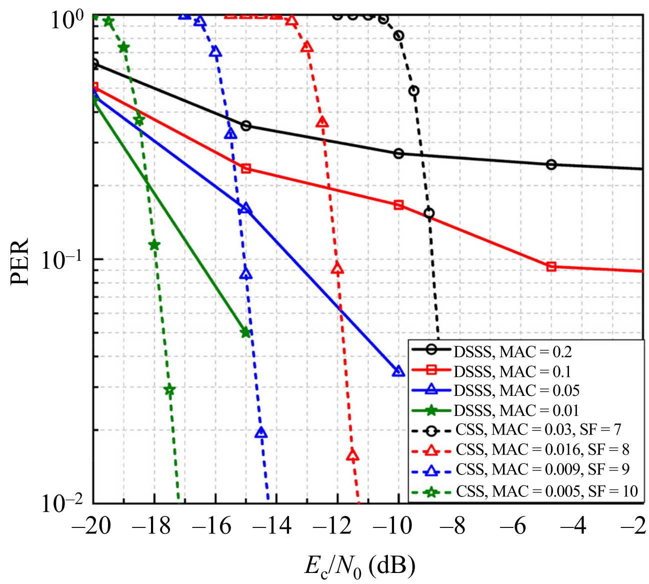

FIGURE 5 Packet error rate (PER) performance of direct sequence spread spectrum (DSSS) with media access control (MAC) load = [0.01, 0.05, 0.1, 0.2] and chirp spread spectrum (CSS) with MAC load = [0.03, 0.016, 0.009, 0.005] corresponding to spreading factor (SF) = [7, 8, 9, 10]

relevant IoT transmission schemes, such as DSSS and CSS, which are considered in this paper. Finally, the link budget can be calculated on the basis of the difference between P_r and P_{req}. To compare the performances of DSSS- [15,19] and CSS-based [5,17] IoT transmission schemes in LEO satellite communication systems, the simulation parameters presented in Table 2 were used to ensure the link margin was over 5 dBm. In satellite communication systems, it considers typically the link margin of a few dB to endure the extra losses owing to rain attenuation or other external factors, for example, implementation loss and interference among multiple terminals.

On the basis of (6) and (7) and Tables 1 and 2, the received powers can be obtained as $P_r = -128.51$ dBm, $P_{req} = -133.61$ dBm for DSSS, and $P_{req} = -134.02$ dBm for CSS. Using these parameter settings, we were able to obtain link margins of 5.1 dBm and 5.51 dBm for DSSS and CSS, respectively. For higher link margins, DSSS and CSS can have the additional gains of 3 dBm and 2.5 dBm by doubling the SFs, respectively. For example, the link margin in DSSS with SF = 9 is 8.1 dBm and the link margin in CSS with SF = 13 is 8.51 dBm. However, the SF values should be properly selected because it can impact greatly the implementation complexity.

3.3 | Performance analysis

Here, we compared the two waveforms under the same bandwidth, E_c/N_0, payload length, code rate, and chip rate conditions. The symbol rate could be calculated as the chip rate divided by the number of chips per symbol. The symbol rates for DSSS and CSS were obtained as 0.976 ksps and 61 sps, respectively. In addition, the E_b/N_0 values of the DSSS and CSS schemes were computed as 7 dB and 8.34 dB, respectively, on the basis of the same $E_c/N_0 = -20$ dB, using the following equations: $E_b/N_0 = E_c/N_0 + 10\log_{10}(2^{SF}) - 10\log_{10}(r)$ for DSSS [4] and $E_b/N_0 = E_c/N_0 + 10\log_{10}(2^{SF}) - 10\log_{10}(SF \times r)$ for CSS [17]. In case of Table 2 for link margin of 5 dB of two transmission schemes, the E_b/N_0 for DSSS is lower than that of CSS, meaning the energy efficiency of DSSS is better than that of CSS. This is because CSS uses a larger number of chips per bit than DSSS for same link margin.

Using the simulation parameters from Tables 1 and 2, we then analyzed the performance of the DSSS and CSS schemes in terms of PER, throughput, and PLR. These measurement indicators are defined as throughput $= \lambda(nD - nE)/(nD + nMD)$, PER $= nE/nD$, and PLR $= (nE + nMD)/(nD + nMD)$, where nD, nMD, and nE refer to the number of detected packets, the missed detected packets, and the error packets among the detected packets, respectively, and λ is the MAC load defined as the amount of transmitted data that has arrived on a certain channel. As the PER represents only the error rate according to the detected packets, there is a limit in determining the initial detection probability. By measuring the performance of the PLR, which reflects the missed detection probability of transmitted packets, we were able to analyze the advantages and disadvantages of DSSS and CSS schemes for LEO satellite IoT systems. To measure the performance, in this simulation, the cell coverages in Figure 3A range from the relative latitude $\gamma = [-25^\circ : 1^\circ : 25^\circ]$ to the relative longitude $\psi = [-25^\circ : 1^\circ : 25^\circ]$. The normalized Doppler shift per cell is calculated from (2). As a result, it has the scope of $[-2.3 \times 10^{-5} \sim 2.3 \times 10^{-5}]$ as shown in Figure 4B. This Doppler shift is equally applied to the multiple uplink signals from terminals located in same cell. However, the E_c/N_0 and MAC load affects only the noise component and interference component, respectively.

Figure 5 shows the PER performances of the DSSS and CSS transmission schemes with different E_c/N_0 values. The PERs of the DSSS scheme were measured with MAC load = [0.01, 0.05, 0.1, 0.2]. As the MAC load increased, the PER increased owing to increasing interference among packets. To guarantee a PER under 0.1 for stable IoT transmission, the DSSS curves of MAC load = [0.01, 0.05, 0.1] are located in E_c/N_0 regions above [−17, −13, −5] dB, respectively. In other words, the DSSS scheme had to have a MAC load under 0.1. For comparison with the DSSS scheme, the PERs of the CSS scheme were measured with SF = [7, 8, 9, 10] instead of MAC load. To guarantee a PER under 0.1, the CSS curves of SF = [7, 8, 9, 10], which can be computed as MAC load = [0.03, 0.016, 0.009, 0.005], are located in E_c/N_0 regions above [−9, −12, −15, −18] dB, respectively. Therefore, the CSS scheme had to have a MAC load under 0.03. This value is remarkably low compared with the maximum MAC load of the DSSS scheme (0.1), verifying the motivation behind the fact that LoRa physical layer is not designed for applications in which many terminals are active simultaneously. In addition, the PER curve of each SF steeply declined in the CSS scheme, as this scheme is less sensitive to noise.

In addition to PER performance, the throughput and PLR are shown in Figures 6 and 7, respectively, for MAC loads equal to or less than 0.1, which satisfy PERs below 0.1 for $E_c/N_0 = [-5, -10, -15, -20]$ dB. First, Figure 6 shows that the throughput of DSSS increases as the MAC load increases. At the same time, the throughput of CSS increases when the MAC load is less than 0.06 and decreases when the MAC load is greater than 0.06. Compared with the DSSS scheme, the CSS scheme shows a high throughput when the MAC load is low and a low

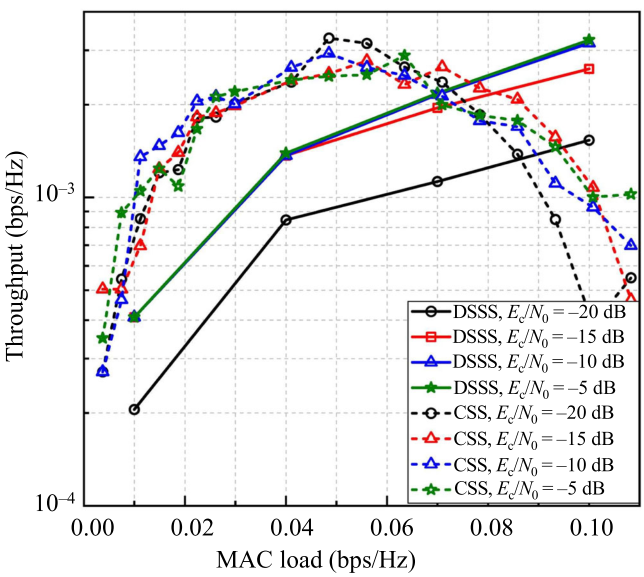

FIGURE 6 Throughput performance of direct sequence spread spectrum (DSSS) and chirp spread spectrum (CSS) with E_c/N_0 = [−5, −10, −15, −20] dB in media access control (MAC) load region under 0.1 for packet error rate (PER) under 0.1

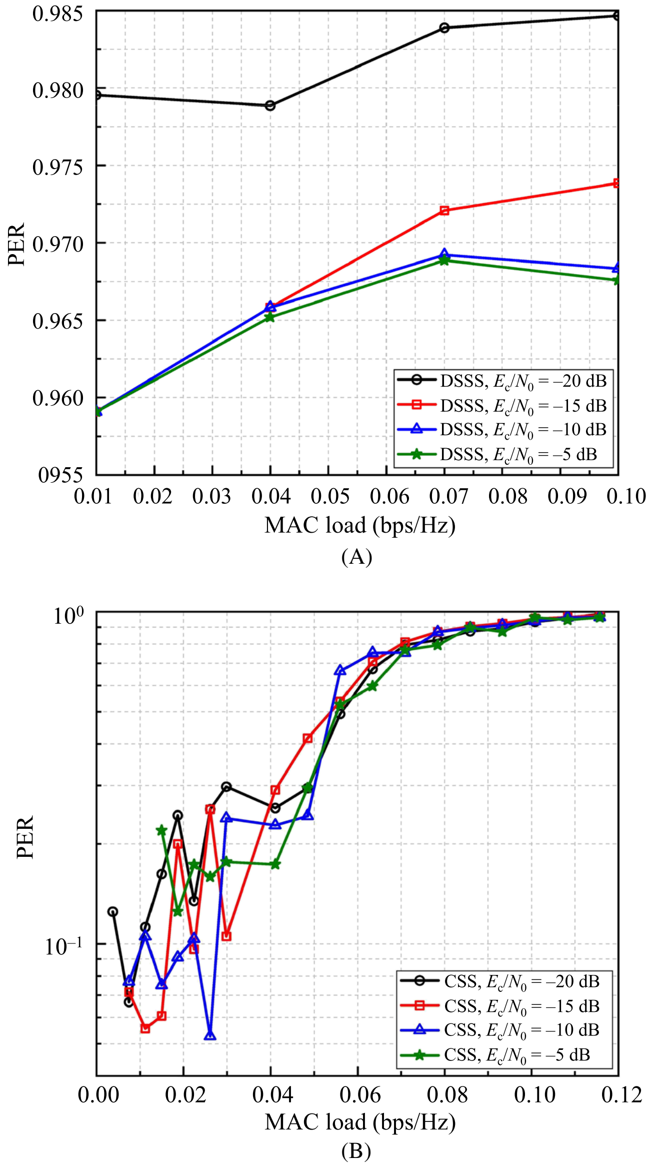

FIGURE 7 Packet loss rate (PLR) performance of (A) direct sequence spread spectrum (DSSS) and (B) chirp spread spectrum (CSS) with E_c/N_0 = [−5, −10, −15, −20] dB in media access control (MAC) load region under 0.1 for packet error rate (PER) under 0.1

throughput when the MAC load is high. In the low-MAC load region, the co-channel interference among packets does not occur frequently. Therefore, the CSS scheme can show superior performance compared with the DSSS scheme under low-traffic conditions owing to its robustness against the Doppler shift. In contrast, the DSSS scheme has higher throughput than the CSS scheme in heavy interference environments. For $E_c/N_0 = -20$ dB, the DSSS scheme showed a particularly substantial decrease in throughput compared with the other E_c/N_0 conditions. This is because it is difficult to detect DSSS packets in the E_c/N_0 range below -20 dB.

To evaluate the packet detection performance of DSSS and CSS receivers, the PLR performance of the two schemes is shown in Figures 7A and 7B, respectively. Figure 7A shows that the PLR value of $E_c/N_0 = -20$ dB is much higher than the PLR value in E_c/N_0 values below -15 dB. This result reflects the opposite tendency compared with the throughput curve of the DSSS scheme shown in Figure 6. The PLR values of the CSS scheme shown in Figure 7B were not influenced by E_c/N_0, as were the throughput curves of CSS in Figure 6. Instead, these PLR curves showed similar performance when E_c/N_0 was larger than the demodulation SNR of -23 dB, which is the SNR sensitivity value of LoRa [25]. In addition, the PLR values of the CSS scheme had very low values at low-MAC loads compared with those of the DSSS scheme because of its robustness against the Doppler effect.

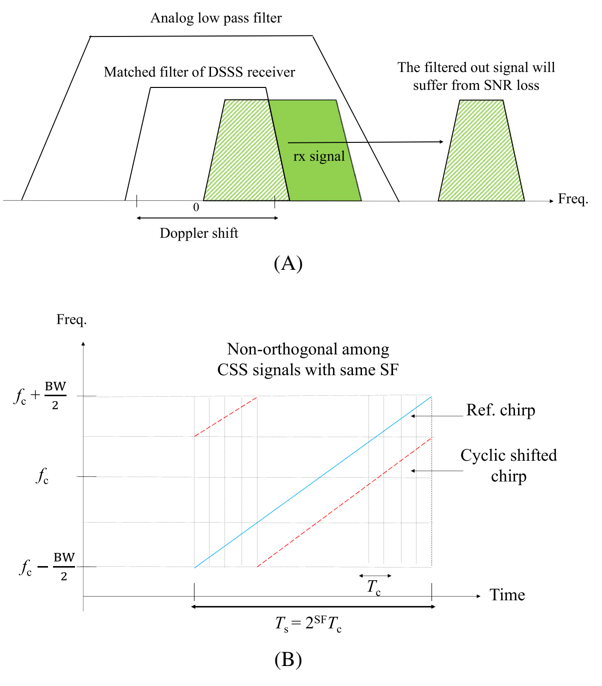

FIGURE 8 Weakness of (A) direct sequence spread spectrum (DSSS) and (B) chirp spread spectrum (CSS) transmission schemes

4 | WAVEFORM ENHANCEMENT FOR SATELLITE IOT

Through various simulation results, we analyzed the strengths and weaknesses of DSSS and CSS schemes in IoT transmission over LEO satellite. The DSSS-based satellite IoT transmission scheme was found to be more suitable than the CSS scheme for high-traffic IoT services, thanks to its robustness against co-channel interference. However, it is essential to remove the performance degradation caused by the Doppler effect to provide IoT services using this transmission scheme. Therefore, this section describes several performance enhancement techniques including preprocessing of the Doppler effect. At the same time, the CSS-based satellite IoT transmission scheme was found to be more suitable than the DSSS scheme for high-mobility IoT services. However, as CSS is very vulnerable to packet collisions, it needs to improve throughput performance to become a strong candidate for IoT transmission services. This paper proposes two solutions that reduce the possibility of packet collision and enhance the physical layer of CSS scheme. The weaknesses of the DSSS and CSS schemes are illustrated in Figure 8A and 8B, respectively. Figure 8A shows that the received signal in the DSSS receiver is largely beyond the boundary for matched filtering by Doppler frequency shift, and the filtered-out signal suffers from SNR loss. In Figure 8B, the reference chirp and the chirp cyclic shifted by $4T_c$ increases linearly in frequency during the symbol period $T_s = 2^{SF}T_c$. It means that the CSS scheme is very weak to packet collisions owing to the nonorthogonal arrangement among CSS signals with the same SF.

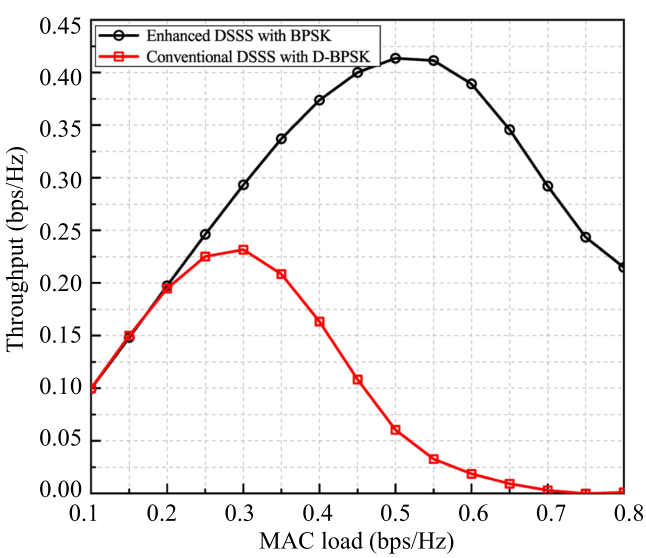

FIGURE 9 Performance comparison of the conventional direct sequence spread spectrum (DSSS) with differential binary phase-shift keying (D-BPSK) and the enhanced DSSS with BPSK

4.1 | DSSS enhancement

To enhance the DSSS-based IoT transmission scheme, two methods are suggested in this paper: changing the modulation type and preprocessing the Doppler effect. These two methods lead to remarkable performance differences compared with other methods, such as using a new preamble pattern, using a long preamble, and changing the channel coding.

4.1.1 | Change of modulation type

The DSSS scheme, based on the IEEE 802.15.4k LECIM standard, avoids the possibility of phase ambiguity using differential encoding that performs an operation of the modulo-2 addition of a raw data bit with the previous encoded bit. However, the DSSS receivers cannot perform phase tracking because they detect the difference in successive phase rather than the absolute phase. Therefore, the use of D-BPSK should suffer a large performance loss of approximately -3 dB unless an iterative decoder is implemented in combination with the convolutional code. To solve this problem, the receiver can adopt a BPSK modulation with a phase tracking function as an alternative to D-BPSK.

Figure 9 shows the throughput performance of the enhanced DSSS scheme by applying BPSK instead of D-BPSK. We measured throughput performance under different MAC loads at $E_b/N_0 = 10$ dB, excluding channel impairments such as shadowing and Doppler effects. The enhanced DSSS has a maximum throughput of 0.41 bps/Hz at a MAC load = 0.5, and the conventional DSSS has a maximum throughput of 0.23 bps/Hz at a MAC load = 0.3, which is approximately double. Instead, the enhanced DSSS receivers should compensate for the distorted phase through a phase tracking process.

4.1.2 | Preprocessing of Doppler effect

In the previous simulation results, shown in Figures 5 to 7, we confirm the DSSS scheme's weakness against the Doppler effect. The DSSS receiver certainly has difficulty in the initial preamble detection owing to the Doppler effect caused by the high speed of LEO satellites. Figure 7A reveals a high PLR for a low-MAC load. To provide IoT transmission service over LEO satellites via DSSS, the elimination of the Doppler effect needs to be considered.

The Doppler shift can be precompensated with estimation from downlink signals or postcompensated with estimation from uplink signals at a gateway placed in an onboard processor (OBP) satellite [15,26]. This paper excludes the postcompensation scheme for the Doppler effect because it is limited to OBP satellites and the estimation accuracy is poor due to the limited header length of DSSS frame [4], whereas the precompensation scheme can be implemented for any types of satellites. In the beacon-based precompensation schemes, downlink beacon signals are used to estimate the Doppler shifts. The beacon signals are periodically transmitted by LEO satellites and may convey ephemeris-related information, such as the satellite position based on its trajectory and absolute time. In IoT terminals with GPS modules, the Doppler shift in the coverage area can be calculated using the satellite position and time information obtained from the received beacon. However, much energy consumption by the GPS modules can be a burden for the IoT terminals that should operate with low power.

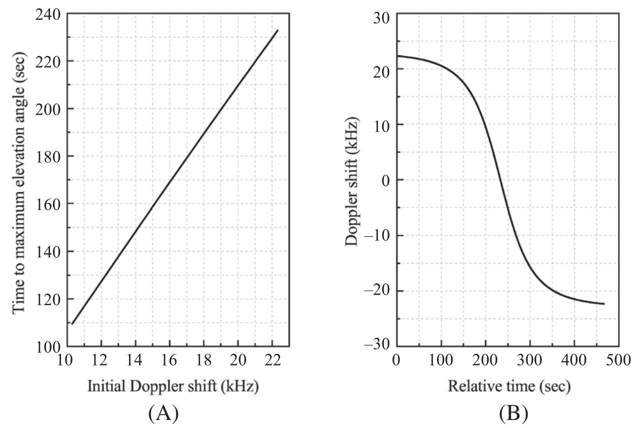

FIGURE 10 Look-up tables (LUT) used for Doppler shift estimation. (A) LUT1: Time to maximum elevation angle after the initial beacon is received. (B) LUT2: Doppler shifts versus the relative time when the maximum elevation angle is 90°

Motivated by this, the downlink beacon-based Doppler effect precompensation scheme without GPS modules is proposed using two LUTs: LUT1 for the estimation of the maximum elevation angle and LUT2 for estimating the Doppler shift as shown in Figure 10. This scheme has the advantage of low power via operating without a GPS module and the future Doppler shift values can be predicted by building two LUTs. Therefore, it results in precise estimation performance. However, the precompensation scheme of Fanfani and others [26] as the reference is impossible to predict the future Doppler shift, and the estimated value through the previous beacon is applied as the next beacon estimate, resulting in performance degradation. The proposed Doppler effect precompensation scheme is composed of three phases: (i) LUT generation phase where two LUTs are generated by the ephemeris information of satellites, (ii) initial estimation phase where the effective regions of LUTs are determined and initial Doppler shift is estimated, and (iii) fine estimation phase where the

Doppler shifts are finely estimated with accumulated beacon signals. The overall process is performed as follows:

Begin **LUT generation phase**: Assume that the satellite flies over the circular orbit at the altitude of H_s with the angular velocity v_a, and the terminal is located where $\theta_{max} = 90°$.

Step 1.1. Time from the minimum elevation angle θ_{min} to the. maximum elevation angle θ_{max} for various inclined orbits is measured.

Step 1.2. LUT1 maps the initial Doppler shift, that is, the Doppler shift at the minimum elevation angle, to the time from the minimum to maximum elevation angles.

Step 1.3. LUT2 is generated by calculating the Doppler shifts as $f_d = v_t f_c / c$ every T_{res} seconds where v_t is the velocity to the terminal.

End **LUT generation phase**

Begin **Initial estimation phase**: The first beacon is received.

Step 2.1. Estimate the initial Doppler shift $\widehat{f}_d^0$ using a preamble from the received beacon.

Step 2.2. Find the time t_{max} for the maximum elevation angle corresponding to the initial Doppler shift from LUT1.

Step 2.3. Determine the window $(t_{ref} - t_{max}, t_{ref} + t_{max})$ for reference Doppler offset in LUT2 using the time obtained from Step 2.2.

Step 2.4. Calculate the error between the initial Doppler shift and the Doppler shift at the start point in the window.

$$e^0 = \widehat{f}_d^0 - \mathrm{LUT2}(t_{ref} - t_{max}). \tag{8}$$

Step 2.5. Estimate the Doppler shift of the second beacon using the error and time period T_b of the beacon.

$$\widetilde{f}_d^1 = \mathrm{LUT2}(t_{ref} - t_{max} + T_b) + e^0. \tag{9}$$

End **Initial estimation phase**

Begin **Fine estimation phase**: The second beacon is received.

Step 3.1. Estimate the Doppler shift $\widehat{f}_d^n$ using the preamble from the received second beacon.

Step 3.2. Calculate the error between the result value of Step 2.5 and the result value of Step 3.1.

$$e^n = \widehat{f}_d^n - \widetilde{f}_d^n. \tag{10}$$

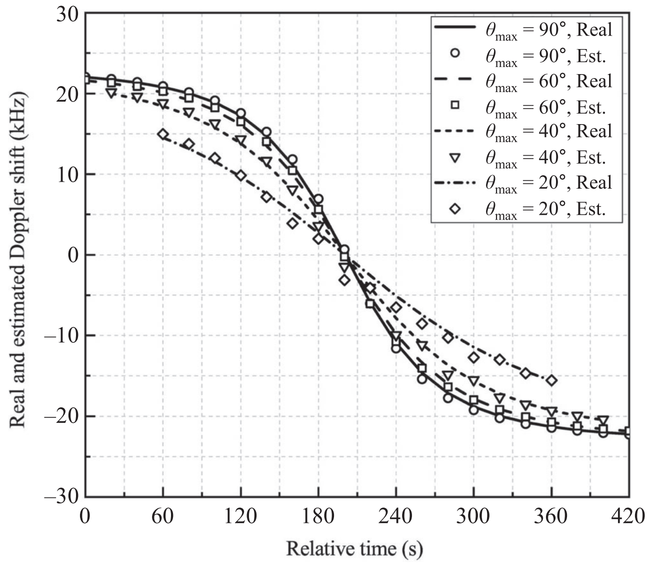

FIGURE 11 Real and estimated Doppler shifts versus the relative time for various maximum elevation angles $\theta_{max} = \{20, 40, 60, 90\}°$

TABLE 3 Simulation environments for Doppler estimation

Parameters	Values
Speed of light, c	3×10^5 km/s
Radius of the Earth, R_E	6378 km
Center frequency, f_c	900 MHz
Altitude, H_s	600 km
Angular velocity, v_a	0.001185 rad/s
Minimum elevation angle, θ_{min}	10°
LUT time resolution, T_{res}	0.1 s
Beacon period, T_b	20 s

Step 3.3. Estimate the Doppler shift of the next beacon using the error and time period of the beacon.

$$\widetilde{f}_d^{n+1} = \mathrm{LUT2}(t_{ref} - t_{max} + (n+1)T_b) + \sum_{i=0}^{n} e^i. \tag{11}$$

Step 3.4. Perform Steps 3.1–3.3 repeatedly.

End **Fine wstimation phase**

Figure 11 shows the real and estimated Doppler shifts versus the relative time for various maximum elevation angle $\theta_{max} = \{20, 40, 60, 90\}°$ based on the parameters in Table 3. For different maximum elevation angles, the estimated Doppler shifts are close to the real values. Because the LUT2 is generated with the maximum

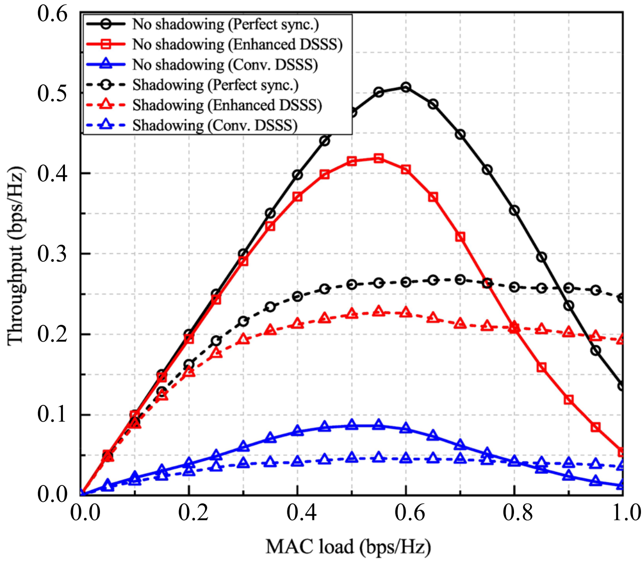

FIGURE 12 Performance comparison of the conventional direct sequence spread spectrum (DSSS) and enhanced DSSS with preprocessing of Doppler effect under the shadowing and no-shadowing environment

elevation angle $\theta_{max} = 90^\circ$, the precompensation scheme performs better than other maximum elevation angles. The accuracy of the estimation would be better with many LUTs for different maximum elevation angles, but there is a tradeoff between the cost caused by memory size and estimation accuracy.

Figure 12 shows the performance comparison of the enhanced DSSS with preprocessing of the Doppler effect and the conventional DSSS in shadowing and no-shadowing environments. It also presents the throughput of perfect synchronization as a reference performance. The channel environment is considered to include a Rician fading of K factor 100 dB and a shadowing effect of −3 dB mean and 3 dB variance in $E_b/N_0 = 10$ dB. Two receiver options are available for performance measurement: perfect synchronization and real reception. In perfect synchronization, the receiver knows in advance the detection position and channel impairments of each burst, whereas the real receiver operates on its own to detect the burst and estimate the channel impairments. In channels without shadowing, the throughput performance under the perfect synchronization conditions increased at MAC loads below 0.6 and decreased at MAC loads above 0.6. Overall, it had the highest throughput of 0.5 bps/Hz at MAC load of 0.6. In addition, the maximum throughputs of the enhanced DSSS and conventional DSSS were approximately 0.1 and 0.4 bps/Hz lower than the reference curve, respectively. At the same time, the throughput performance in the shadowing channel was considerably degraded compared with that of the no-shadowing channel. In all cases, the maximum throughput was reduced by about half. Similarly, the maximum throughputs of the enhanced DSSS and conventional DSSS were approximately 0.05 and 0.2 bps/Hz lower than the reference curve in the shadowing channel, respectively. These results show that large-scale fading, such as shadowing, is the most dominant factor in terms of throughput performance, whereas the Doppler shift is the second largest cause of degradation.

We also considered other methods to improve performance, such as using a new preamble pattern, using a longer preamble, and changing the channel coding. First, we applied the turbo code instead of the convolutional code of the IEEE 802.15.4k standard. The turbo code can be performed very close to the capacity limit using two recursive convolutional encoders [27]. Second, we used other preamble sequences, including Zadoff–Chu and Bjorck sequences [28–30], instead of the binary sequence of the IEEE 802.15.4k standard. Finally, a long preamble was used to increase the initial detection probability. Despite all these efforts, the throughput performance improved slightly owing to the high complexity burden. Therefore, we excluded their use because of the inefficiency of these methods.

4.2 | CSS enhancement

4.2.1 | Avoidance of packet collision

To enhance the CSS-based IoT transmission scheme, we propose a solution to improve throughput performance on the basis of lowering the probability of packet collision. Running LoRa on satellite channels can cause conflicts with many terminals transmitting signals. Further, it is difficult to detect the signals transmitted by other terminals owing to interference from packet collisions. This is because each terminal using the same SF has a nonorthogonal property as shown in Figure 8B. As a result, the throughput is considerably reduced. Therefore, each terminal should determine which SF to transmit the desired information so as to avoid collision. Until now, the selection of SFs used in CSS-based terminals has generally been made with equal probability. This approach limits the throughput performance. In this paper, we formulated a simple optimization problem to maximize the throughput by selecting the appropriate probability that each device will use SFs when using a pure ALOHA random access scheme.

Supposing a scenario in which N terminals transmit signals to the same satellite, and each terminal transmits k bits of information to the satellite, the number of symbols N_{syms} according to the LoRa standard when using the SFs i is given by

$$N_{\text{syms}} = 12 + \left\lceil \frac{k}{i} \right\rceil. \tag{12}$$

When the bandwidth used by the LoRa signals is BW, the length of a packet using the SFs i is given by

$$T_i = N_{\text{syms}} \times \frac{2^i}{\text{BW}}. \tag{13}$$

Since all terminals operate in a distributed manner, the probability that each terminal uses SFs i is defined in $p_i, \sum_i p_i = 1, i \in \{7, 8, 9, 10, 11, 12\}$. Further, we assume that the MAC load λ of data transferred by each terminal follows a Poisson distribution. Assuming that each device has the same MAC load, the probability that packets with the same SF will not collide is given by

$$P_{\text{non\_collision},i} = \exp(-p_i N \lambda T_i). \tag{14}$$

On the basis of (14), the total throughput of each device can be given by

$$\Gamma = \sum_{i=7}^{12} p_i \lambda P_{\text{non\_collision},i}. \tag{15}$$

The optimization problem for maximizing throughput is formulated as follows:

$$\begin{aligned} &\max_{\substack{p_i \\ i \in \{7,8,9,10,11,12\}}} \quad \Gamma \\ &\text{s.t.} \ \sum_{i=7}^{12} p_i = 1, \ \forall i, \ 0 \le p_i \le 1. \end{aligned} \tag{16}$$

The above expression can be easily solved with an optimization problem solver using the interior-point method. MATLAB R2020a Optimization Toolbox was used as a solver in the present simulation. The parameters for simulation were set to $k = 100$, $\text{BW} = 125\,\text{kHz}$, $N = 5$, and the number of symbols for preamble and synchronization was 12. The resulting

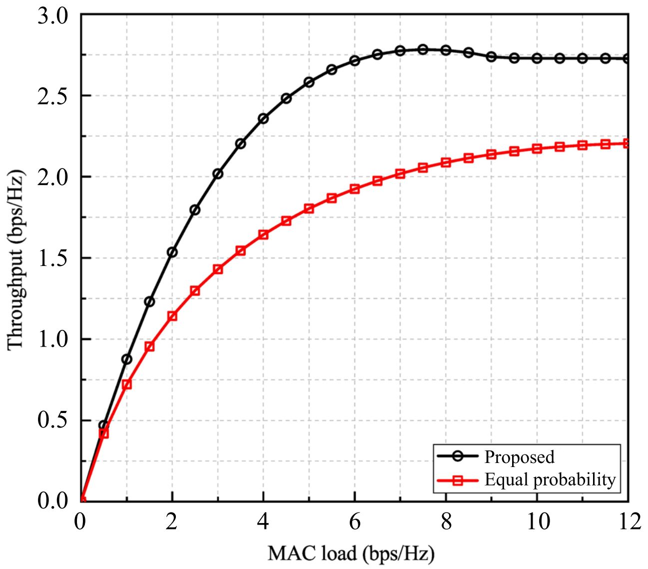

FIGURE 13 Throughput performance of the proposed scheme and equal probability scheme with different MAC loads

TABLE 4 Statistics for real detection scenario (conventional chirp spread spectrum [CSS])

E_c/N_0	Detected packets	Missed detected packets	False alarms	Error packets
−26 dB	0	9998	0	0
−25 dB	56	9942	0	41
−24 dB	2181	7817	0	954
−23 dB	8686	1313	1	1224
−22 dB	9993	6	0	215

TABLE 5 Statistics for real detection scenario (enhanced chirp spread spectrum [CSS])

E_c/N_0	Detected packets	Missed detected packets	False alarms	Error packets
−26 dB	0	9998	0	0
−25 dB	51	9947	0	0
−24 dB	2187	7811	0	0
−23 dB	8711	1288	1	0
−22 dB	9990	9	0	0

packet lengths $T_{i \in \{7,8,9,10,11,12\}}$ were set to [0.0276, 0.0512, 0.0983, 0.1802, 0.3604, 0.6881] s for SFs from 7 to 12, respectively. For comparison, we simulated a case using the same probability for each SF. Figure 13 shows the throughput performance of the proposed scheme with an optimization problem solver and the equal probability scheme with different MAC loads. It can be seen that the proposed scheme significantly improved the throughput performance over the case in which all bandwidths had the same probability of being used.

4.2.2 | Enhancement on physical layer

To improve the overall block error rate (BLER) performance of CSS scheme, we propose an enhanced physical layer structure of the conventional CSS scheme: extending the number of preamble symbols to improve packet detection probability as well as changing the coding scheme from hamming code to convolutional code. Tables 4 and 5 is the statistics for real detection scenario in case of SF = 12 of conventional and enhanced CSS examined by our simulator, respectively. The conventional CSS uses (8, 4) hamming code and the enhanced CSS uses convolutional code with $r = 1/2$ and constraint length 7.

Table 4 shows the number of detected packets, missed detected packets, false alarms, and error packets of conventional CSS for $E_c/N_0 = [-26, -25, -24, -23, -22]$ dB. Almost all performance degradation is owing to missed detection in the low SNR range. Moreover, even if

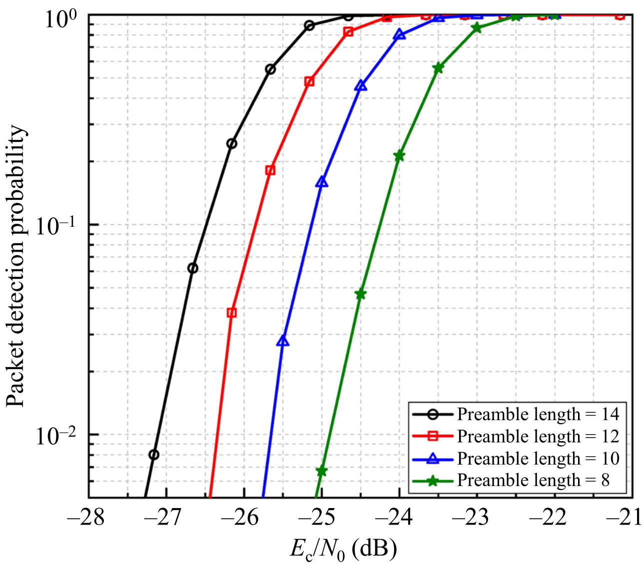

FIGURE 14 Packet detection probability of enhanced chirp spread spectrum (CSS) scheme with preamble length = [8, 10, 12, 14] in case of spreading factor (SF) = 12

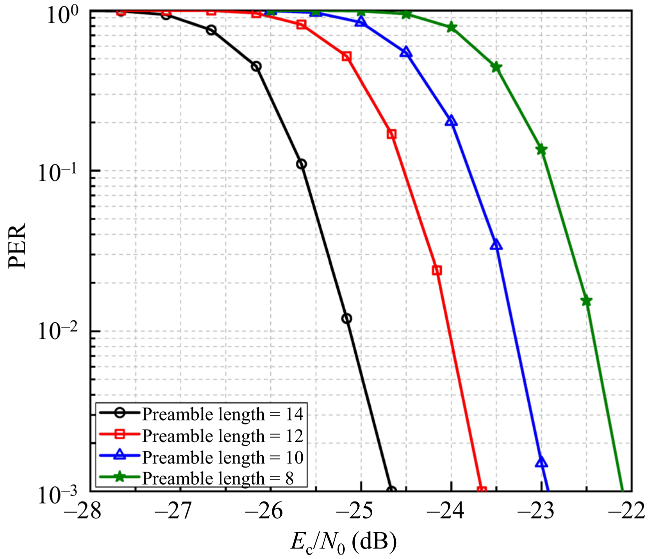

FIGURE 15 Packet error rate (PER) performance of enhanced chirp spread spectrum (CSS) scheme with preamble length = [8, 10, 12, 14] in case of spreading factor (SF) = 12

packet detection is well-performed in the high SNR range, the packet error somewhat occurs. To improve the PER performance, first, we change the coding scheme from (8, 4) hamming code to convolutional code with $r = 1/2$ because (8, 4) hamming code is little coding gain [31]. Table 5 shows the statistics of the enhanced CSS using convolutional code with $r = 1/2$ like Table 4. By changing coding scheme, packet error is substantially reduced. However, the performance degradation caused by packet loss remains an issue.

By extending preamble length, the packet detection probability and PER can be enhanced as shown in Figures 14 and 15, respectively. In both Figures 14 and 15, it shows that SNR gain is greater than 2 dB by increasing the number of preamble symbols from 8 to 14 in case of SF = 12.

So far, this paper has independently analyzed each performance of enhanced DSSS and CSS in terms of throughput. To prove the validity of the proposed methods, performance comparison between the proposed methods and the latest methods is required. First, enhanced DSSS scheme shows a throughput of almost 0.1 bps/Hz at MAC load = 0.1 in Figure 12. That is, all terminal signals can be accurately transmitted and received by precompensating the Doppler effect in the LEO satellite environment for low-traffic service. In Kim and others [15], it presents the throughput of DSSS transmission scheme using ideal genie-aided receiver, which can estimate perfectly the Doppler shift, in LEO satellite environment considering various channel impairments. Compared with the throughput of [15], this paper shows an almost close performance in the low-traffic region.

This result proves that the enhanced DSSS scheme has as good performance as the genie-aided receiver assuming ideal detection and synchronization. At this time, the simulation conditions are almost the same except for the frequency band that uses the 2.4 GHz S-band instead of 900 MHz considered in this paper. Next, to compare the two enhanced schemes in the same environment, the throughput of the enhanced CSS scheme can be calculated in (16) by considering approximately 2600 terminals corresponding to the LEO satellite cell coverage of Figure 3A. As a result, it shows a throughput of approximately 0.015 bps/Hz at MAC load = 0.1. However, the existing scheme of selecting the SFs used in CSS-based terminals with equal probability has a throughput of about 0.01 bps/Hz when the MAC load is 0.1 using (15). The proposed approach using the optimization problem solver performs slightly better than using equal probability in low-traffic regions. In addition, compared with the enhanced DSSS scheme, the enhanced CSS scheme shows approximately seven times lower throughput. This is because LoRa can use a limited number of different SFs from 7 to 12. In conclusion, it can be confirmed that the enhanced DSSS is more suitable for both the high-traffic and high-mobility services than the enhanced CSS compared with the previous results, in which DSSS is suitable for high-traffic service and CSS is suitable for high-mobility service.

5 | CONCLUSIONS

In this paper, we undertook a performance comparison between LoRa based on a CSS scheme and Ingenu based on a DSSS scheme for IoT transmission over LEO satellites. The performance in terms of the PER, throughput, and PLR was measured in a channel environment considering the Doppler effect caused by the high speed of LEO satellites and the interference among multiple terminals. On the basis of the simulation results, we concluded that the DSSS scheme is more suitable than the CSS scheme for IoT services with high traffic because of its robustness against interference among multiple terminals. At the same time, the CSS scheme was found to be more suitable than the DSSS scheme for IoT services with high mobility because of its robustness against frequency offset. To enhance the DSSS transmission scheme, it is proposed to change the modulation type and eliminate the Doppler effect. In particular, a precompensation scheme without GPS modules was applied using two LUTs to estimate the Doppler effect. This method shows the low-power consumption and precise estimation performance. To enhance the CSS transmission scheme, we proposed two solutions: avoidance of packet collision and enhancement on physical layer. Among them, a load distribution scheme is applied to lower the probability of packet collision. To distribute the load, CSS-based terminals selected SFs with an optimization problem solver. As a result of the simulation, the proposed DSSS and CSS enhancement techniques significantly improved performance, and among them, the enhanced DSSS scheme is more suitable for both high-traffic and high-mobility services than the enhanced CSS scheme.

FUNDING INFORMATION

This work was supported by Institute of Information and Communications Technology Planning and Evaluation (IITP) grant funded by the Korea government (MSIT) (No. 2020-0-00843, Development of low-power satellite multiple access core technology based on LEO cubesat for global IoT service)

ORCID

Sooyeob Jung https://orcid.org/0000-0001-8763-3844

REFERENCES

1. 3GPP TS 36.211 v.14.3.0, *LTE: Evolved universal terrestrial radio access (E-UTRA); physical channels and modulation (Release 14)*, 2017.
2. Semtech, *LoRa Modem Design Guide: SX1272/3/6/7/8/9*, 2020, available at https://www.semtech.com/
3. Sigfox, *Sigfox Technology*, 2020. available at https://www.sigfox.com/
4. IEEE Standard, *IEEE standard for local and metropolitan area networks—Part 15.4: Low-rate wireless personal area networks (LR-WPANs), Amendment 5: Physical layer specifications for low energy, critical infrastructure monitoring networks*, 2013.
5. C. C. Chan, A. Al-Hourani, J. Choi, K. M. Gomez, and S. Kandeepan, *Performance modeling framework for IoT-over-satellite using shared radio spectrum*, MDPI Remote Sens **12** (2020), no. 10. https://doi.org/10.3390/rs12101666
6. 3GPP TR 38.811 v.0.1.0, *Study on new radio (NR) to support non-terrestrial networks (Release 15)*, 2017.
7. Y. S. Song, S. K. Lee, J. W. Lee, D. W. Kang, and K. W. Min, *Analysis of adjacent channel interference using distribution function for V2X communication systems in the 5.9-GHz band for ITS*, ETRI J. **41** (2019), no. 6, 703–714.
8. H. Zhang, X. Chu, W. Guo, and S. Wang, *Coexistence of Wi-Fi and heterogeneous small cell networks sharing unlicensed spectrum*, IEEE Commun. Mag. **53** (2015), no. 3, 158–164.
9. Ingenu, *RPMA: Technology for the Internet of Things*, 2015, available at https://www.ingenu.com
10. A. Ikpehai, B. Adebisi, K. M. Rabie, K. Anoh, R. E. Ande, M. Hammoudeh, H. Gacanin, and U. M. Mbanaso, *Low-power wide area network technologies for internet-of-things: A comparative review*, IEEE IoT J. **6** (2019), no. 2, 2225–2240.
11. J. P. Queralta, T. N. Gia, Z. Zou, H. Tenhunen, and T. Westerlund, *Comparative study of LPWAN technologies on unlicensed bands for M2M communication in the IoT: Beyond LoRa and LoRaWAN*, in Proc. Int. Conf. Future Netw. Commun. (Halifax, Canada), Aug. 2019, pp. 343–350.

12. Y. Qian, L. Ma, and X. Liang, *Symmetry chirp spread spectrum modulation used in LEO satellite Internet of Things*, IEEE Commun. Lett. **22** (2018), no. 11, 2230–2233.
13. Y. Qian, L. Ma, and X. Liang, *The performance of chirp signal used in LEO satellite Internet of Things*, IEEE Commun. Lett. **23** (2019), no. 8, 1319–1322.
14. US7773664 B2, *Random phase multiple access system with meshing*, 2010.
15. P. Kim, S. Jung, D. H. Jung, J. G. Ryu, and D. G. Oh, *Performance analysis of direct sequence spread spectrum aloha for LEO satellite based IoT service*, in Proc. IEEE Veh. Technol. Conf. (Honolulu, HI, USA), Sept. 2019, pp. 1–5.
16. A. Berni and W. Gregg, *On the utility of chirp modulation for digital signaling*, IEEE Trans. Commun. **21** (1973), no. 6, 748–751.
17. G. Ferré and A. Giremus, *LoRa physical layer principle and performance analysis*, in Proc. IEEE Int. Conf. Electron. Circuits Syst. (Bordeaux, France), Dec. 2018, pp. 65–68.
18. A. O. Afisiadis, A. Burg, and A. Balatsoukas-Stimming, *Coded LoRa frame error rate analysis*, in Proc. IEEE Int. Conf. Commun. (Dublin, Ireland), June 2020, pp. 1–6.
19. Y. Tada and S. Kato, *A star-topology sensor network system for agriculture using 802.15.4K standard*, in Proc. IEEE Personal, Indoor Mobile Radio Commun. (London, UK), June 2013, pp. 76–80.
20. 3GPP TR 36.763 v1.0.0, *3GPP; technical specification group radio access network; study on narrow-band Internet of Things (NB-IoT) /enhanced machine type communication (eMTC) support for non-terrestrial networks (NTN) (Release 17)*, 2021.
21. I. Ali, N. Al-Dhahir, and J. Hershey, *Doppler characterization for LEO satellites*, IEEE Trans. Commun. **46** (1998), no. 3, 309–313.
22. B. Vucetic and J. Du, *Channel modeling and simulation in satellite mobile communication systems*, IEEE J. Selected Areas Commun. **10** (1992), no. 8, 1209–1218.
23. L. M. Davis, I. B. Collings, and R. J. Evans, *Estimation of LEO satellite channels*, in Proc. IEEE Int. Conf. Inform., Commun. Sig. Process. (Singapore), Sept. 1997. https://doi.org/10.1109/ICICS.1997.647048
24. Y. Roth, *The physical layer for low power wide area networks: A study of combined modulation and coding associated with an iterative receiver*, July 2017, available at HAL Id: tel-01568794. https://hal.archives-ouvertes.fr/tel-01568794v1
25. B. Laporte-Fauret, M. A. Temim, G. Ferré, D. Dallet, B. Minger, and L. Fuché, *An enhanced LoRa-Like receiver for the simultaneous reception of two interfering signals*, in Proc. IEEE Personal, Indoor Mobile Radio Commun. (Istanbul, Turkey), Sept. 2019. https://doi.org/10.1109/PIMRC.2019.8904258
26. A. Fanfani, S. Morosi, L. Ronga, and E. Del Re, *Frequency recovery techniques for TM/TC satellite modem in critical scenarios*, Int. J Satell. Commun. Netw. **36** (2017), no. 36, 179–193.
27. B. Tahir, S. Schwarz, and M. Rupp, *BER comparison between convolutional, Turbo, LDPC, and polar codes*, in Proc. IEEE Int. Conf. Telecommun. (Limassol, Cyprus), May 2017. https://doi.org/10.1109/ICT.2017.7998249
28. I. Stankovic, C. Ioana, and M. Dakovic, *Sequence comparison in reconstruction and targeting in underwater sonar imaging*, in Proc. IEEE OCEANS (Marseille, France), 2019. https://doi.org/10.1109/OCEANSE.2019.8867478
29. J. Bendetto and J. Donatelli, *Ambiguity function and frame-theoretic properties of periodic zero-autocorrelation waveforms*, IEEE J. Sel. Top. Signal Process. **1** (2007), no. 1, 6–20.
30. A. Kebo, I. Konstantinidis, J. J. Benedetto, M. R. Dellomo, and J. M. Sieracki, *Ambiguity and sidelobe behavior of CAZAC coded waveforms*, in Proc. IEEE Radar Conf. (Waltham, MA, USA), 2007. https://doi.org/10.1109/RADAR.2007.374198
31. T. Elshabrawy and J. Robert, *Evaluation of the BER performance of LoRa communication using BICM decoding*, in Proc. IEEE Int. Conf. Consumer Electron. (Berlin, Germany), Sept. 2019. https://doi.org/10.1109/ICCE-Berlin47944.2019.8966172

AUTHOR BIOGRAPHIES

Sooyeob Jung received a BS degree in electrical engineering and computer science from Kyungpook National University, Daegu, Republic of Korea, in 2009, and an MS degree in electrical engineering from the Korea Advanced Institute of Science and Technology (KAIST), Daejeon, South Korea, in 2011. He is currently pursuing a PhD degree at KAIST. In 2011, he joined the Electronics and Telecommunications Research Institute (ETRI), Daejeon, Republic of Korea. His research interests include digital satellite communication systems, optimization for wireless communications, and modem technology.

Gyeongrae Im received a BSE degree from KAIST, Daejeon, Republic of Korea, in 2013, and a PhD degree in electrical and computer engineering from Seoul National University, Seoul, Republic of Korea, in 2019. Since 2019, he has been working at ETRI, Daejeon, Republic of Korea. His research interests include future 6G wireless communication systems, satellite communication systems, and information theory-based wireless communication systems.

Dong-Hyun Jung received BS and MS degrees in electrical engineering from Pohang University of Science and Technology (POSTECH), Pohang, Republic of Korea and Seoul National University, Seoul, Republic of Korea, in 2015 and 2017, respectively. He is currently pursuing a PhD degree in electrical engineering at KAIST, Daejeon, Republic of Korea and working as a researcher at ETRI, Daejeon, Republic of Korea. His research interests include stochastic geometry-based analyses and satellite communication.

Pansoo Kim received BS and MS degrees in electrical and computer engineering from Sungkyunkwan University, Suwon, Republic of Korea, in 2000 and 2002, respectively. Since 2002, he has been with ETRI, Daejeon, Republic of Korea, as a principal researcher. His research field is transmission technologies related to satellite communication and telecommunication systems.

Joon Gyu Ryu received BS, MS, and PhD degrees in radio and information communications engineering from Chungnam National University, Daejeon, Republic of Korea, in 1999, 2001, and 2014, respectively. Since 2001, he has been working ETRI, Daejeon, Republic of Korea, as a principal researcher. His research interests include satellite broadcasting and communication systems and RF technology.

Joonhyuk Kang (Member, IEEE) received BSE and MSE degrees from Seoul National University, Seoul, Republic of Korea, in 1991 and 1993, respectively, and a PhD degree in electrical and computer engineering from The University of Texas at Austin, Austin, TX, USA, in 2002. From 1993 to 1998, he was a Research Staff Member with Samsung Electronics, Suwon, Republic of Korea, where he was involved in the development of DSP-based real-time control systems. He was with Cwill Telecommunications, Austin, in 2000, where he participated in the project for multi-carrier CDMA systems with antenna arrays. From 2008 to 2009, he was a Visiting Scholar at the School of Engineering and Applied Sciences, Harvard University, Cambridge, MA, USA. He is currently working as the Head of the School of Electrical Engineering, KAIST, Daejeon, Republic of Korea. His research interests include signal processing for cognitive radio, cooperative communication, physical-layer security, and wireless localization. He is a member of the Korea Information and Communications Society and the Tau Beta Pi (the Engineering Honor Society). From 2000 to 2002, he was a recipient of the \Texas Telecommunication Consortium Graduate Fellowship.

How to cite this article: S. Jung, G. Im, D.-H. Jung, P. Kim, J. G. Ryu, and J. Kang, *Performance analysis of DSSS- and CSS-based physical layer for IoT transmission over LEO satellites*, ETRI Journal (2022), 1–17. https://doi.org/10.4218/etrij.2021-0038